

# Fast Resonance Assignment and Fold Determination of Human Superoxide Dismutase by High-Resolution Proton-Detected Solid-State MAS NMR Spectroscopy\*\*

Michael J. Knight, Amy L. Webber, Andrew J. Pell, Paul Guerry, Emeline Barbet-Massin, Ivano Bertini, Isabella C. Felli, Leonardo Gonnelli, Roberta Pierattelli, Lyndon Emsley, Anne Lesage, Torsten Herrmann, and Guido Pintacuda\*

The field of protein solid-state NMR spectroscopy has recently made impressive technical and methodological progress, opening up several new prospects in the analysis of an increasingly larger range of systems in many areas of modern structural biology.<sup>[1]</sup>

Solution-state structural investigations of proteins traditionally use the detection of protons, which, with their high gyromagnetic ratio, usually provide the best possible sensitivity,<sup>[2]</sup> whereas for fully protonated samples in the solid state the large homonuclear  $^1\text{H}$  dipolar couplings result in linewidths that are prohibitive to constructive use. For this reason, solid-state NMR studies of biomolecules are traditionally performed by directly detecting  $^{13}\text{C}$  which has lower sensitivity due to the smaller gyromagnetic ratio, but significantly higher resolution. However, it has been shown that the use of perdeuterated proteins makes solid-state proton detection feasible by diluting the proton dipolar network.<sup>[3]</sup> Using moderate magic-angle spinning (MAS) rates (10–20 kHz), it has been shown that extremely high proton resolution can be obtained using partially back-exchanged amide sites, in samples typically prepared in 10%  $\text{H}_2\text{O}$  and 90%  $\text{D}_2\text{O}$ .<sup>[4]</sup> Nonetheless,  $^1\text{H}$ - $^1\text{H}$  contacts, which are a rich source of information for the determination of a 3D structure,

can be probed more efficiently in samples at higher protonation levels.<sup>[5]</sup> For example, an optimal back-exchange level of 25% was used for the structure calculation of SH3 using amide and methyl  $^1\text{H}$ - $^1\text{H}$  restraints in combination with dihedral restraints from chemical shifts.<sup>[6]</sup> Similarly, the combination of partial back-exchange with selectively protonated methyl groups has been applied to the structure calculation of ubiquitin, using methyl  $^1\text{H}$ - $^1\text{H}$  restraints together with dihedral restraints.<sup>[7]</sup> The compromise between resolution and sensitivity has been shown to be different at higher MAS rates, and for example complete amide protonation has been used in the case of the model domains GB1<sup>[8]</sup> and SH3<sup>[9]</sup> at 40 and 60 kHz MAS, respectively. In this respect a significant advantage has been provided recently by the development of MAS probes capable of spinning small-diameter rotors at ultra-fast frequencies ( $> 50$  kHz). Under ultra-fast MAS, spin dynamics are profoundly altered; the  $^1\text{H}$  dipolar couplings are heavily weakened and, in addition, the use of low-power irradiation for heteronuclear decoupling<sup>[10]</sup> and selective CP<sup>[11]</sup> is facilitated. Cumulatively, these factors open the way to the analysis of more complex biological solids that may be available in very limited amounts.

Here, we show that the use of high magnetic fields, ultra-fast MAS, and 100% NH re-protonation in perdeuterated samples allow extensive assignment and structure determination of medium-sized proteins using  $^1\text{H}$  resonances. Namely, we have applied proton-detected MAS solid-state NMR spectroscopy to the 153-residue microcrystalline dimeric ( $2 \times 16$  kDa)  $\text{Zn}^{\text{II}}$ -loaded superoxide dismutase ( $\text{Zn}^{\text{II}}$ -SOD).<sup>[12]</sup> This system was perdeuterated with uniform [ $^{13}\text{C}$ ,  $^{15}\text{N}$ ]-labeling and fully re-protonated at the exchangeable sites. We have developed experiments for assignment of the backbone  $^1\text{H}$ ,  $^{15}\text{N}$ ,  $^{13}\text{CA}$  and  $^{13}\text{CO}$  resonances under ultra-fast MAS, and determined the fold of  $\text{Zn}^{\text{II}}$ -SOD using a 3D (H)NHH<sub>RFDR</sub> experiment and automated assignment procedures.

Figure 1 shows a  $^1\text{H}$ -detected dipolar HN correlation of [100%  $^1\text{H}^{\text{N}}$ ,  $^1\text{H}$ ,  $^{13}\text{C}$ ,  $^{15}\text{N}$ ]- $\text{Zn}^{\text{II}}$ -SOD at high magnetic field (corresponding to a Larmor frequency of 1 GHz for  $^1\text{H}$ ) and ultra-fast MAS (60 kHz). These experimental conditions guarantee relatively long  $^1\text{H}$  coherence lifetimes (of the order of 10 ms) with typical apparent linewidths of the order of 100 Hz (0.1 ppm at 23.5 T). In this spectrum, 110 resonances are fully resolved.

The above HN correlation provides a quick fingerprint of the molecule similarly to the widely employed scalar-coupling

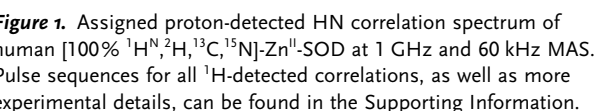
[\*] Dr. M. J. Knight, Dr. A. L. Webber, Dr. A. J. Pell, Dr. P. Guerry, E. Barbet-Massin, Prof. L. Emsley, Dr. A. Lesage, Dr. T. Herrmann, Dr. G. Pintacuda

Centre de RMN à Très Hauts Champs, UMR 5280 CNRS/Ecole Normale Supérieure de Lyon, University of Lyon  
5 rue de la Doua, 69100 Villeurbanne (France)  
E-mail: guido.pintacuda@ens-lyon.fr  
Homepage: www.ens-lyon.fr/crmn

Prof. I. Bertini, Prof. I. C. Felli, Dr. L. Gonnelli, Prof. R. Pierattelli  
Department of Chemistry "Ugo Schiff" and Magnetic Resonance Center (CERM), University of Florence  
via Luigi Sacconi 6, 50019 Sesto Fiorentino FI (Italy)

[\*\*] We acknowledge support from the Agence Nationale de la Recherche (ANR 08-BLAN-0035-01 and 10-BLAN-713-01), from Ente Cassa di Risparmio di Firenze, from Egide (programme Galilée 22397R), from the Università Italo-francese (programma Galileo 09/10) and from Joint Research Activity and Access to Research Infrastructures in the 7th Framework program of the EC (BioNMR n. 261863).

Supporting information for this article (full experimental procedures about sample preparation, solid-state  $^1\text{H}$  detected NMR spectra acquisition and structure calculation, and the list of the assigned shifts and  $^1\text{H}$ - $^1\text{H}$  contacts) is available on the WWW under <http://dx.doi.org/10.1002/anie.201106340>.



Here, a suite of four 3D experiments was designed, combining the HN dipolar correlation module with  $^{13}\text{C}$ - $^{15}\text{N}$  and  $^{13}\text{C}$ - $^{13}\text{C}$  specific transfers (Figure 2a–c). These sequences yield correlations where the  $i^{\text{th}}$  amide  $^1\text{H}$  and  $^{15}\text{N}$  shifts are correlated to either the  $^{13}\text{CO}$  or the  $^{13}\text{CA}$  shifts, in either the same  $i^{\text{th}}$  or the preceding  $(i-1)^{\text{th}}$  residue. Note that, at this level of amide re-protonation, CP is generally more efficient than through-bond INEPT for transferring coherences between  $^1\text{H}$  and  $^{15}\text{N}$ , or between  $^{15}\text{N}$  and  $^{13}\text{C}$ , while INEPT has a comparable efficiency to dipolar-based methods for the  $^{13}\text{C}$ - $^{13}\text{C}$  transfers.<sup>[14]</sup> Sequential assignment of the backbone resonances is then obtained from the alignment of strips from the spectra. A representative portion of this sequential walk is

**Figure 2.** a–c) Pulse sequences used for proton-detected sequential assignment experiments. a) (H)CONH/(H)CANH; b) (H)CO(CA)NH; c) (H)CA(CO)NH. Narrow and broad black rectangles indicate  $90^\circ$  and  $180^\circ$  pulses, respectively, the bell shapes represent band-selective  $\pi$ -pulses, and the delay  $\tau$  is set to  $1/4J$  (4.7 ms for  $J_{\text{COCA}} = 53$  Hz). More details are available in the Supporting Information. d) Representative strips from proton-detected assignment of human [100%  $^1\text{H}$ ,  $^2\text{H}$ ,  $^{13}\text{C}$ ,  $^{15}\text{N}$ ]-Zn-SOD at 1 GHz and 60 kHz MAS: (H)CONH, (H)CO(CA)NH (blue and black contours of the upper plot, respectively), (H)CANH, (H)CA(CO)NH (black and blue contours of the lower plot, respectively). Sequential correlations are marked by the red line.

**(a)** Pulse sequence for 1H, 15N, and 13CO/13CA channels. 1H channel includes phases  $\Phi_1$ , CP, sITPPM, and  $\Phi_3$ . 15N channel includes phases  $\Phi_1$ , CP,  $t_2$ ,  $\tau_{sat}$ ,  $\Phi_2$ , CP, and WALTZ-16. 13CO/13CA channel includes phases  $\Phi_1$ , CP,  $t_1$ , CP, and WALTZ-16.

**(b)** Pulse sequence for 1H, 15N, and 13CO channels. 1H channel includes phases  $\Phi_1$ , CP, sITPPM, and  $\Phi_3$ . 15N channel includes phases  $\Phi_1$ , CP,  $t_2$ ,  $\tau_{sat}$ ,  $\Phi_2$ , CP, and WALTZ-16. 13CO channel includes phases  $\Phi_1$ , CP,  $t_1$ , CP, and WALTZ-16.

**(c)** Pulse sequence for 1H, 15N, and 13CA channels. 1H channel includes phases  $\Phi_1$ , CP, sITPPM, and  $\Phi_3$ . 15N channel includes phases  $\Phi_1$ , CP,  $t_2$ ,  $\tau_{sat}$ ,  $\Phi_2$ , CP, and WALTZ-16. 13CA channel includes phases  $\Phi_1$ , CP,  $t_1$ , CP, and WALTZ-16.

**(d)** 2D NMR spectra for residues I112, I113, G114, R115, T116, and L117. The x-axis is  $\delta(^{15}\text{N})$  / ppm (116.9, 121.5, 113.0, 118.5, 112.5, 129.6) and the y-axis is  $\delta(^{13}\text{C})$  / ppm (170, 175, 45, 50, 55, 60). The spectra show peaks for (H)CONH, (H)CO(CA)NH, (H)CANH, and (H)CA(CO)NH.

in solution-state NMR spectroscopy.<sup>[15]</sup> Notably, this yields an assignment independently from previously available solution data, which is often a prerequisite for the study of solid-state samples of this size.<sup>[16]</sup>  $^1\text{H}$ ,  $^{15}\text{N}$ ,  $^{13}\text{CO}$ , and  $^{13}\text{CA}$  shifts of a total of 145 residues (out of 147 non-proline residues) were assigned this way (see Supporting Information).

Having assigned the amide resonances, the quality of the HN fingerprint can conveniently be exploited in order to determine  $^1\text{H}$ - $^1\text{H}$  distance restraints. We therefore conducted a 3D (H)NHH<sub>RFDR</sub> experiment,<sup>[6,8]</sup> where  $^1\text{H}$ - $^1\text{H}$  RFDR mixing<sup>[17]</sup> was used to correlate nearby proton spins, and  $^{15}\text{N}$  editing used to provide good resolution, superficially similar to the solution-state HSQC-NOESY.<sup>[18]</sup>

Example strips from this experiment are shown in Figure 3a. Note that the experiment is easily extensible to higher dimensionality, which for larger systems may be necessary to

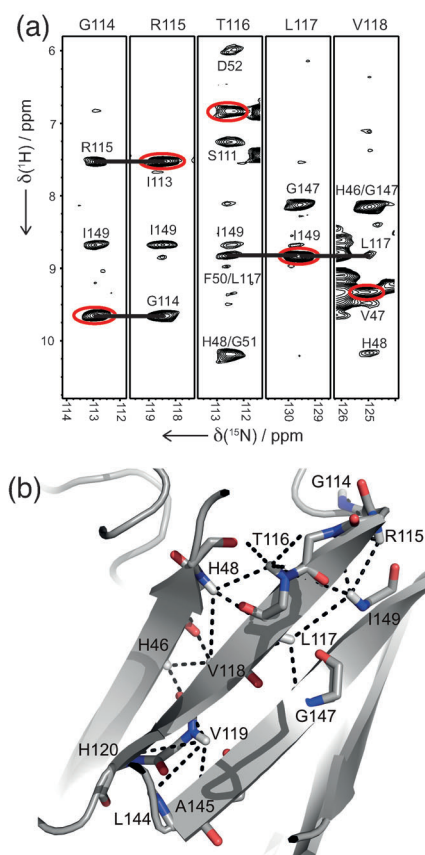


**Figure 3.** a) Strips from the proton-detected (H)NHH<sub>RFDR</sub> experiment (3.3 ms mixing time). The diagonal peak in each strip is circled, whilst solid lines indicate trivial contacts ( $|i-j| = 1$ ) which were not used in the structure calculation. b) The long-range contacts detected in a) are depicted on the crystal structure of the  $\text{Cu}^{\text{II}}, \text{Zn}^{\text{II}}$ -SOD homologue.

overcome potential limitations of resolution and resultant ambiguity.<sup>[7]</sup> Here, the resolution and sensitivity of the 3D map enables cross-peak analysis and structure calculation by using automatic tools such as the ATNOS/CANDID<sup>[19]</sup> procedure implemented in the NMR data analysis software suite UNIO.<sup>[20]</sup>

Chemical shift guided peak-picking of the (H)NHH<sub>RFDR</sub> spectrum was performed by ATNOS.<sup>[19]</sup> In the first assign-

ment and structure calculation cycle (of seven) carried out by ATNOS/CANDID, a filtering protocol making use of a homologous structure ( $\text{Cu}^{\text{II}}, \text{Zn}^{\text{II}}$ -SOD, PDB code: 1SOS<sup>[21]</sup>) was used. This was employed to discard artifacts (noise) mistaken for peaks in the spectrum that were not consistent with any realistic assignment (any possible proton pairs up to 8 Å apart), and to ensure that, in the first cycle, assignments consistent with the homologous structure were not erroneously discarded. However, all other initial chemical shift-based assignment possibilities for each cross-peak compatible with the network-anchored assignment filter<sup>[19]</sup> were maintained. Thus at the outset the algorithm generated a self-consistent set of ambiguous distance restraints for calculating an initial fold. The UNIO protocol then used multiple cycles of concerted assignment and structure calculation, with each cycle guiding the subsequent stages. Notably, distance bin ranges for cross-peak volumes were not implemented in the manner typically used for solution-state NOESY data, since the cross-peak volume when using variants of spin diffusion (here with RFDR recoupling) is a complex function of internuclear distance and topology.<sup>[22]</sup> Here, cross-peaks volumes were converted into upper distance bounds by using a local grid search approach for finding all compatible conformers with an internally generated dihedral restraint list derived from  $^1\text{H}$ ,  $^{15}\text{N}$  and  $^{13}\text{CO}/^{13}\text{CA}$  shifts,<sup>[23]</sup> and during all cycles no homologous structure was needed for assigning the cross peaks, for calibrating their volumes against  $^1\text{H}$ - $^1\text{H}$  distances, or for structure calculation.

A significant number (192) of unique, non-trivial distance restraints useful for structure determination could be extracted from the (H)NHH<sub>RFDR</sub> experiment. Typically, for strips corresponding to residues in  $\beta$ -sheets, cross-peaks are observed which are assignable to inter-strand contacts, beside the trivial sequential contacts (Figure 3b). In total, 72 of the assigned contacts were “medium-range” (between residues  $i$  and  $j$  with  $3 \leq |i-j| \leq 5$ ) and 120 long-range (between residues  $i$  and  $j$  with  $|i-j| > 5$ ); about 20 contacts correspond to  $^1\text{H}$  pairs with a separation of more than 6 Å. The structural information provided by the amide  $^1\text{H}$ - $^1\text{H}$  contacts was sufficient to define the secondary structure elements and their relative positions into the 3D fold of the monomeric unit of  $\text{Zn}^{\text{II}}$ -SOD, resulting in a bundle with backbone root-mean-square deviation (RMSD) of 1.64 Å (Figure 4). The average structure backbone RMSD to the X-ray structure is 2.34 Å, for residues in regular secondary structure elements.

These results further demonstrate the advantages provided by perdeuterated samples at high re-protonation levels.<sup>[8,9]</sup> Particularly, we note that, to gain this level of structural insight for a protein of this size by using lower levels of re-protonation, the sensitivity of the 3D HH experiment would decrease quadratically. Low levels of re-protonation appear to make larger samples volumes a necessity, requiring more protein, and different experimental protocols.<sup>[6]</sup>

This result represents a substantial step forward in biomolecular solid-state NMR spectroscopy, since the use of  $^1\text{H}$ -based structure restraints allowed here the use of automated structure calculation in solid-state NMR for a system significantly larger than those for which such approaches have thus far been applied. It must be noted that, for protein chains



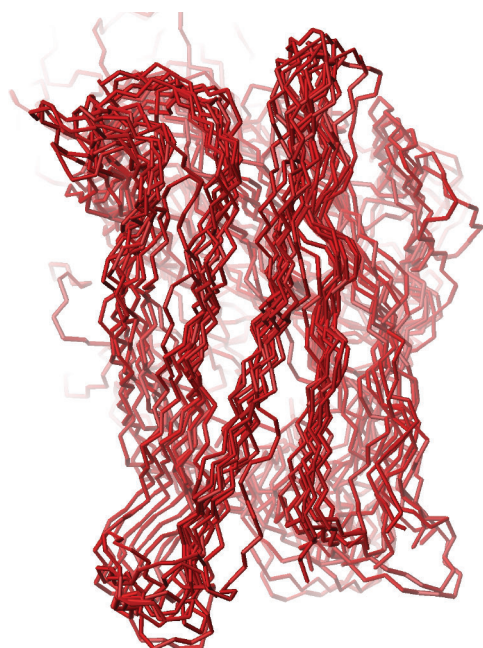


**Figure 4.** Structure ensemble for Zn<sup>II</sup>-SOD determined by <sup>1</sup>H-detected solid-state NMR.

longer than about 100 residues, <sup>13</sup>C-<sup>13</sup>C maps such as those provided by, for example, proton-driven spin diffusion (PDSF) experiments on protonated samples at lower MAS rates yield highly ambiguous contacts, which are thus difficult to convert into meaningful restraints.<sup>[24]</sup> The availability of a rapidly determined backbone fold can be further used to guide the interpretation of different experimental restraints, allowing subsequent refinement stages. Based upon the present result, it is to be anticipated that de novo solid-state NMR structures of large proteins at very high resolution may be calculable.

In conclusion, we have shown that <sup>1</sup>H-detected solid-state NMR spectroscopy at high magnetic fields and ultra-fast MAS can be readily and usefully applied to amide resonance assignment and structure determination of a protein of considerable size. Less than 4 mg (0.25 μmol) of protein was used in this study, and remarkably short experimental times were needed to assign <sup>1</sup>H resonances and to detect amide proton–proton distance restraints. A total of 8 days of measurement time was required for all the <sup>1</sup>H-detected experiments described in this work, inclusive of pulse sequence calibration.

We believe that these results will contribute significantly in increasing the impact of solid-state NMR spectroscopy in structural biology, in particular as deuteration and back-substitution of exchangeable protons has recently been shown to yield high-quality proton-detected spectra for a variety of heterogeneous systems. These include fibrils formed by the Alzheimer's disease β-amyloid peptide Aβ<sub>40</sub>, the lipid reconstituted β-barrel membrane protein OmpG, and the α-helical membrane protein bacteriorhodopsin.<sup>[25]</sup>

Received: September 7, 2011  
Published online: October 13, 2011

**Keywords:** <sup>1</sup>H detection · NMR spectroscopy · protein structure · structural constraints

- [1] a) A. E. McDermott, *Annu. Rev. Biophys.* **2009**, *38*, 385–403; b) C. Wasmer, A. Lange, H. Van Melckebeke, A. B. Siemer, R. Riek, B. H. Meier, *Science* **2008**, *319*, 1523–1526; c) S. Jehle, P. Rajagopal, B. Bardiaux, S. Markovic, R. Kühne, J. R. Stout, V. A. Higman, R. E. Klevit, B. J. van Rossum, H. Oschkinat, *Nat. Struct. Mol. Biol.* **2010**, *17*, 1037–1042.
- [2] a) Y. Ishii, J. P. Yesinowski, R. Tycko, *J. Am. Chem. Soc.* **2001**, *123*, 2921–2922; b) E. K. Paulson, C. R. Morcombe, V. Gaponenko, B. Dancheck, R. A. Byrd, K. W. Zilm, *J. Am. Chem. Soc.* **2003**, *125*, 15831–15836; c) M. Hologne, V. Chevelkov, B. Reif, *Prog. Nucl. Magn. Reson. Spectrosc.* **2006**, *48*, 211–232.
- [3] B. Reif, C. P. Jaroniec, C. M. Rienstra, M. Hohwy, R. G. Griffin, *J. Magn. Reson.* **2001**, *151*, 320–327.
- [4] V. Chevelkov, K. Rehbein, A. Diehl, B. Reif, *Angew. Chem.* **2006**, *118*, 3963–3966; *Angew. Chem. Int. Ed.* **2006**, *45*, 3878–3881.
- [5] U. Akbey, S. Lange, T. W. Franks, R. Linser, K. Rehbein, A. Diehl, B. J. van Rossum, B. Reif, H. Oschkinat, *J. Biomol. NMR* **2010**, *46*, 67–73.
- [6] R. Linser, B. Bardiaux, V. Higman, U. Fink, B. Reif, *J. Am. Chem. Soc.* **2011**, *133*, 5905–5912.
- [7] M. Huber, S. Hiller, P. Schanda, M. Ernst, A. Böckmann, R. Verel, B. H. Meier, *ChemPhysChem* **2011**, *12*, 915–918.
- [8] a) D. H. Zhou, G. Shah, M. Cormos, C. Mullen, D. Sandoz, C. M. Rienstra, *J. Am. Chem. Soc.* **2007**, *129*, 11791–11801; b) D. H. Zhou, J. J. Shea, A. J. Nieuwkoop, W. T. Franks, B. J. Wylie, C. Mullen, D. Sandoz, C. M. Rienstra, *Angew. Chem.* **2007**, *119*, 8532–8535; *Angew. Chem. Int. Ed.* **2007**, *46*, 8380–8383.
- [9] J. R. Lewandowski, J. N. Dumez, U. Akbey, S. Lange, L. Emsley, H. Oschkinat, *J. Phys. Chem. Lett.* **2011**, *2*, 2205–2211.
- [10] a) S. Laage, J. R. Sachleben, S. Steuernagel, R. Pierattelli, G. Pintacuda, L. Emsley, *J. Magn. Reson.* **2009**, *196*, 133–141; b) V. Vijayan, J. P. Demers, J. Biernat, E. Mandelkow, S. Becker, A. Lange, *ChemPhysChem* **2009**, *10*, 2205–2208.
- [11] S. Laage, A. Marchetti, J. Sein, R. Pierattelli, H. J. Sass, S. Grzesiek, A. Lesage, G. Pintacuda, L. Emsley, *J. Am. Chem. Soc.* **2008**, *130*, 17216–17217.
- [12] R. W. Strange, S. V. Antonyuk, M. A. Hough, P. A. Doucette, J. S. Valentine, S. S. Hasnain, *J. Mol. Biol.* **2006**, *356*, 1152–1162.
- [13] T. Igumenova, A. J. Wand, A. E. McDermott, *J. Am. Chem. Soc.* **2004**, *126*, 5323–5331.
- [14] a) R. Linser, U. Fink, B. Reif, *J. Magn. Reson.* **2008**, *193*, 89–93; b) R. Linser, U. Fink, B. Reif, *J. Biomol. NMR* **2010**, *47*, 1–6.
- [15] a) M. Ikura, L. E. Kay, A. Bax, *Biochemistry* **1990**, *29*, 4659–4667; b) M. Sattler, J. Schleucher, C. Griesinger, *Prog. Nucl. Magn. Reson. Spectrosc.* **1999**, *34*, 93–158.
- [16] a) G. Pintacuda, N. Giraud, R. Pierattelli, A. Böckmann, I. Bertini, L. Emsley, *Angew. Chem.* **2007**, *119*, 1097–1100; *Angew. Chem. Int. Ed.* **2007**, *46*, 1079–1082; b) S. Laage, A. Lesage, L. Emsley, I. Bertini, I. C. Felli, R. Pierattelli, G. Pintacuda, *J. Am. Chem. Soc.* **2009**, *131*, 10816–10817.
- [17] A. E. Bennett, J. H. Ok, R. G. Griffin, S. Vega, *J. Chem. Phys.* **1992**, *96*, 8624–8627.
- [18] D. Marion, P. C. Driscoll, L. E. Kay, P. T. Wingfield, A. Bax, A. Gronenborn, G. M. Clore, *Biochemistry* **1989**, *28*, 6150–6156.
- [19] a) T. Herrmann, P. Güntert, K. Wüthrich, *J. Mol. Biol.* **2002**, *319*, 209–227; b) T. Herrmann, P. Güntert, K. Wüthrich, *J. Biomol. NMR* **2002**, *24*, 171–189.
- [20] a) F. Fiorito, T. Herrmann, F. F. Damberger, K. Wüthrich, *J. Biomol. NMR* **2008**, *42*, 23–33; b) J. Volk, T. Herrmann, K. Wüthrich, *J. Biomol. NMR* **2008**, *41*, 127–138.
- [21] H. E. Parge, R. A. Hallewell, J. A. Tainer, *Proc. Natl. Acad. Sci. USA* **1992**, *89*, 6109–6113.

- [22] B. H. Meier in *Adv. Magn. Opt. Reson.*, Vol. 18 (Ed.: W. S. Warren), Academic Press, New York, **1994**, p. 1.
- [23] T. Manolikas, T. Herrmann, B. H. Meier, *J. Am. Chem. Soc.* **2008**, *130*, 3959–3966.
- [24] a) A. Loquet, B. Bardiaux, C. Gardiennet, C. Blanchet, M. Baldus, M. Nilges, T. Malliavin, A. Böckmann, *J. Am. Chem. Soc.* **2008**, *130*, 3579–3589; b) A. Loquet, C. Gardiennet, A. Böckmann, *C. R. Chim.* **2010**, *13*, 423–430.
- [25] R. Linser, M. Dasari, M. Hiller, V. Higman, U. Fink, J. M. Lopez del Amo, S. Markovic, L. Handel, B. Kessler, P. Schmieder, D. Oesterhelt, H. Oschkinat, B. Reif, *Angew. Chem.* **2011**, *123*, 4601–4605; *Angew. Chem. Int. Ed.* **2011**, *50*, 4508–4512.
-